INORGANIC CHEMISTRY FRONTIERS

RESEARCH ARTICLE

View Article Online
View Journal | View Issue

Cite this: *Inorg. Chem. Front.*, 2022, **9**, 4065

Multifunctional lanthanide MOF luminescent sensor built by structural designing and energy level regulation of a ligand†

Xueguang Liu,‡[a] Wei Liu,*‡[b] Yao Kou,[a] Xiaoshan Yang,[a] Zhenghua Ju[a] and Weisheng Liu *[a]

In order to reduce usage cost and simplify the detection process, it is necessary to develop multifunctional and multi-emitter Ln-MOF luminescent sensors. The structure and property of Ln-MOFs are mainly controlled by ligands. As a typical aromatic nucleus, naphthalene groups not only can emit fluorescence and regulate the energy levels of a ligand but also can participate in π–π stacking. As a type of directional weak interaction, hydrogen bonding interactions have caught wide attention in catalysis, molecular recognition, self-assembly, *etc*. So we designed a "V" shaped ligand containing naphthalene groups and "O=C–NH" groups as guided by DFT calculations. The obtained Eu-MOF can achieve simultaneous luminescence of the ligand and Eu^{3+}. Single crystal X-ray diffraction revealed that π–π stacking interactions and hydrogen bonding interactions played an important role in the crystallization process. The luminescence spectra showed that the Eu-MOF has two luminescent centers and can be developed as a ratiometric luminescent sensor. The luminescence of the Eu-MOF can undergo an obvious color change from red to white as the temperature rises from 120 to 400 K and the Eu-MOF has a satisfactory relative sensitivity and a small temperature uncertainty. Moreover, the Eu-MOF can detect picric acid selectively and the K_{SV} can reach 53 339 M^{-1}. Thus, the Eu-MOF can be used as a multifunctional and multi-emitter luminescent sensor and the designed strategy also can provide inspiration for further research on Eu-MOFs.

Received 21st April 2022,
Accepted 11th June 2022

DOI: 10.1039/d2qi00859a

rsc.li/frontiers-inorganic

Introduction

As a new type of organic and inorganic hybrid material, metal–organic frameworks (MOFs) integrate metal ions and organic ligands by coordinated interactions and have been studied in lots of fields, including gas storage and separation,[1–5] heterogeneous catalysis,[6–10] proton conduction,[11–15] luminescence detection,[16–22] *etc*. MOFs have a huge specific surface area and dense pore channels that can be designed and controlled.

Lanthanide metal–organic frameworks (Ln-MOFs), especially Eu/Tb-MOFs,[23–34] have been developed widely for luminescence and detection because the luminescence behaviors of Eu^{3+} and Tb^{3+} have many advantages due to f–f transitions, such as a relatively fixed emission wavelength, narrow emission peak, larger Stokes shift, *etc*. However, the absorption peaks of Eu^{3+} and Tb^{3+} are too narrow to achieve a higher fluorescence quantum yield. But some organic ligands have a wide absorption spectrum and can transfer energy to Eu^{3+} and Tb^{3+} so that Eu^{3+} and Tb^{3+} can emit stronger luminescence, which is usually called the "antenna effect". Although lots of Eu-MOFs and Tb-MOFs have been studied, the Eu-MOFs involving two luminescent centers lack attention and can be used as ratiometric luminescent sensors which can avoid disturbance from background light. The building strategy of the Eu-MOFs involving two luminescent centers might be divided into two types, including importing luminescent guest molecules into pore channels and importing luminescent centers into ligands.[33] The former might be suitable for most of the Eu-MOFs having the capacity of accommodating guest molecules and might cause decreased porosity, while the latter might maintain integrity of the Eu-MOFs and it might be

[a]*Key Laboratory of Nonferrous Metal Chemistry and Resources Utilization of Gansu Province and State Key Laboratory of Applied Organic Chemistry, Key Laboratory of Special unction Materials and Structure Design, Ministry of Education, College of Chemistry and Chemical Engineering, Lanzhou University, Lanzhou 730000, China. E-mail: liuws@lzu.edu.cn*
[b]*Institute of National Nuclear Industry, Frontiers Science Center for Rare Isotope, School of Nuclear Science and Technology, Key Laboratory of Special Function Materials and Structure Design, Ministry of Education, Lanzhou University, 730000 Lanzhou, China. E-mail: l_w@lzu.edu.cn*

†Electronic supplementary information (ESI) available. CCDC 2158094. For ESI and crystallographic data in CIF or other electronic format see DOI: https://doi.org/10.1039/d2qi00859a

‡These authors contributed equally to this work.

difficult to design suitable ligands. According to our group's experience in designing functional ligands, we decided to design a ligand with fluorescent centers and low excited state levels. Firstly, the shape of the ligand was designed as "V" shaped, which can promote the appearance of diamond channels according to the reported experiences.[35–39] Secondly, a naphthalene molecule was planned to be introduced as an inflection point of the "V" shaped ligand. Naphthalene molecules have more delocalized electrons than benzene rings, causing stronger π*–π transitions and lower excited energy levels. Thus, the introduction of naphthalene molecules might cause an imperfect "antenna effect" so as to achieve simultaneous luminescence of Eu^{3+} and ligands. Besides, naphthalene molecules can achieve π–π stacking, which might help MOFs crystalize smoothly. Then, in order to achieve the relatively large sizes of pore channels, it is common to increase properly the length of ligands. Benzoic acids were thought to be candidates forming the frames of the "V" shaped ligand, originating from the experience and contribution of pioneers. At the same time, in order to increase the function sites of the ligand, "O═C–NH" bonds were considered to link benzoic acids and naphthalene molecules. The reason why the "O═C–NH" bonds were selected as linkers is that they not only can maintain stability in a common environment but also have hydrogen donors and accepters which not only can promote the crystallization of Eu-MOFs by hydrogen bonding interactions but also can be used as active sites for detecting substrate molecules.

Temperature is one of the most fundamental physical parameters and is closely related with physical chemistry and the biological environment. Due to the high relative sensitivity of luminescence detection, more and more Ln-MOFs have been designed as ratiometric luminescence thermometers. Qian, Chen, and their coworkers[40–45] have designed a series of ratiometric luminescence thermometers and elaborated how to evaluate ratiometric luminescence thermometers. The Ln-MOFs that have been designed as ratiometric luminescence thermometers mainly include single-lanthanide and mixed-lanthanide dual-emission MOFs. Our Eu-MOF belongs to the former whose advantages are that the luminescence of ligands can be designed and the energy transfers easily between two luminescent centers. Besides, detection of small molecules was explored. Nitro explosives as a common type of dangerous chemical have caught wide attention, resulting from their harm in the natural environment and terrorist attacks. Picric acid (PA) is one of the most dangerous nitro explosives, so it is necessary to detect PA selectively and quickly.[46–49] As PA has three nitro groups and one hydroxyl group, it is inferred that the Eu-MOF might recognize PA by hydrogen bonding interactions. This assumption was verified by the following experiment.

Based on the above strategy for structural designing and energy level regulation of a ligand, we designed a "V" shaped dicarboxylic acid ligand which can provide structural sites and functional sites, 4,4′-((naphthalene-2,3-diylbis(azanediyl))bis(carbonyl))dibenzoic acid. The Ln-MOF (Ln = Eu, Gd, Tb) was synthesized by the solvothermal method and was found to be isostructural by PXRD analysis. Structural analysis reveals that the Ln-MOF has two types of diamond channels resulting from the surrounding of the "V" shaped ligand and stacking by 2D layers respectively. It should be emphasized that no interpenetration occurs in the stack process and new diamond pore channels occur after stacking. Surprisingly, π–π stacking interactions and hydrogen bonding interactions really work out in the process of crystallization, as proved by the appearance of steady structural units. Fortunately, the Eu-MOF has two luminescent centers including Eu^{3+} and the ligand, which are in accord with our expectation. The thermal luminescence behaviors of the Eu-MOF and the luminescence detection of nitro explosives were studied. Compared with our previous work, the Eu-MOF has been improved in structure design and luminescence detection. Moreover, it is proved that ligand functionalization can effectively introduce two luminescent centers into a single-lanthanide MOF. This work not only achieved the combination of weak interactions but also achieved the combination of two types of luminescent centers by ingenious designing of the ligand, providing precious experience for our work in the future.

Experimental

Synthesis of the ligand

At first, naphthalene-2,3-diamine 1.8960 g (12 mmol) and methyl 4-(chlorocarbonyl)benzoate 4.7522 g (24 mmol) were dissolved in 120 mL dry CH_2Cl_2. Then 4 mL triethylamine (Et_3N) was added dropwise into the mixed solution and the mixture was stirred at 40 °C for 24 h under Ar. The mixture was washed with 1 M HCl solution, water, $NaHCO_3$ saturated solution, and deionized water respectively. The organic phase was dried with concentrated sodium sulfate under reduced pressure. The obtained yellow solid was dissolved in 50 mL CH_3OH and mixed with 5 mL water solution of KOH (1.3 g). The hydrolysis reaction was stirred at 80 °C for 24 h. The mixture was concentrated under reduced pressure and diluted with water until it dissolved completely. The pH of the solution was adjusted to 3 by adding 1 M HCl solution. Finally, a brown solid was obtained by suction filtration and dried. Yield: 4.79 g, (88%). ^{1}H NMR (400 MHz, DMSO): δ 10.49 (s, 2H), 8.24 (s, 4H), 8.06 (s, 4H), 7.89 (s, 2H), 7.46 (s, 2H), 7.07 (s, 2H). ^{13}C NMR (101 MHz, DMSO): δ 167.90, 166.00, 137.92, 136.20, 131.10, 129.84, 128.28, 126.54, 124.33 (Fig. S1 and S2†).

Synthesis of the Eu-MOF

$Eu(NO_3)_3{\cdot}6H_2O$ (0.0446 g, 0.1 mmol) and the ligand (0.0227 g, 0.05 mmol) were dissolved in 4 mL mixed liquid (DMAC/H_2O = 3/1). The mixture was kept at 90 °C for 3 days and cooled gradually to room temperature. Yellow crystals were obtained through filtration and washed with DMAC. [66% yield]. IR (cm^{-1}, KBr): 3421 (m), 3230 (s), 3057 (m), 1956 (w), 1653 (s), 1593 (s), 1531 (s), 1410 (s), 1290 (s), 1173 (m), 1143 (m), 1016 (m), 920 (w), 870 (m), 804 (m), 739 (s), 598 (m), 509 (w)

(Fig. S3†). The phase purity of the Eu-MOF was confirmed by powder X-ray diffraction (PXRD) (Fig. S4†). Eu-MOF CCDC: 2158094.†

Similarly, the Tb-MOF and Gd-MOF were obtained by the above method.

Results and discussion

Structure description

According to single-crystal X-ray diffraction analysis, it is confirmed that the Eu-MOF crystallizes in the monoclinic space group $P2_1/c$ (Table S1†). The asymmetric unit contains three deprotonated ligands, two Eu^{3+} with different coordination environments, one coordinated DMAC molecule and two coordinated H_2O molecules, while the free solvent molecules include three DMAC molecules and one H_2O molecule. As displayed in Fig. 1a, the coordination number of Eu1 is seven and the coordination polyhedron of Eu1 is a single-capped octahedron while the Eu2 having nine coordinated O atoms shows a single hat square inverse prism coordination polyhedron. Besides, Eu2 coordinates with seven oxygen atoms from the deprotonated ligands, two oxygen atoms from H_2O molecules while the Eu1 coordinates with six oxygen atoms from the deprotonated ligands and one DMAC molecule. Moreover, the bond length of Eu–O ranges from 2.340 to 2.647 Å (Table S2†), which is in accordance with the reported europium-oxygen complexes.[47]

Two adjacent Eu1 atoms are linked by four carboxylic acids from ligands and assemble into the second building units (SBU-1, Fig. 1b). Differently, two adjacent Eu2 atoms share two oxygen atoms from ligands and assemble into the Eu_2O_{16} binuclear cluster as the second building units (SBU-2, Fig. 1b). Then, the SBU-1 and SBU-2 line alternately along *a* axis and form Eu–O–C chains (Fig. 1c). And the chains are linked by "V" shaped ligands, causing the appearance of diamond channels (5 Å × 17 Å) and 2D layers (Fig. 1d). Interestingly, every three adjacent ligands along the *a* axis assemble into a stable unit (Fig. 2a) by π–π stacking interactions from adjacent naphthalene groups and hydrogen bonding interactions from adjacent "O=C–NH" groups. The hydrogen bonding interactions are: N–H···O d = 2.744 Å, θ = 149.94°; N–H···O d = 3.047 Å, θ = 159.64°; N–H···O d = 2.976 Å, θ = 175.65°; N–H···O d = 2.764 Å, θ = 153.81°. As reported in the literature,[48] these hydrogen bonding interactions are moderate. And the π–π stacking interactions between naphthalene groups belong to a parallel displaced conformation.[49] The distance between naphthalene groups ranges from 3.694 Å to 4.385 Å, which is in accordance with the reported data. It is not ignored that the

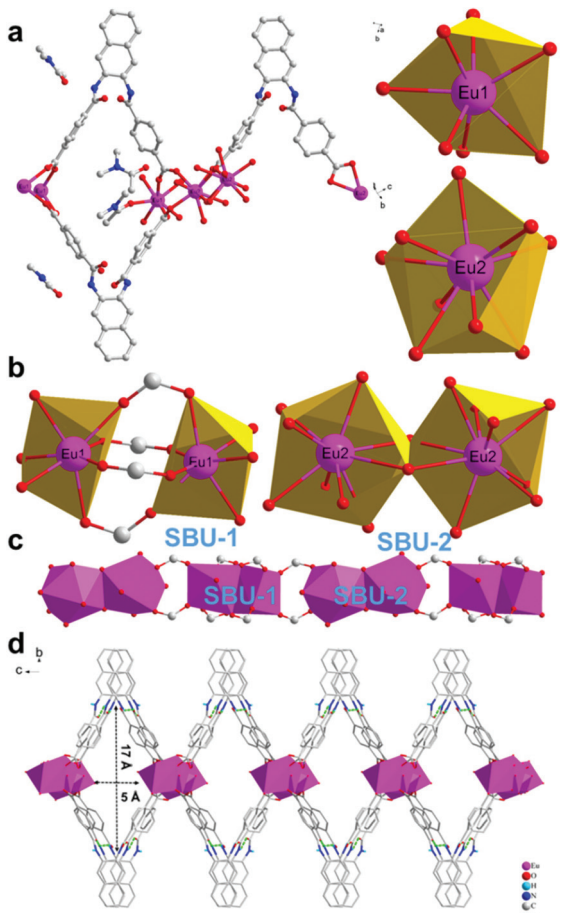

Fig. 1 (a) Coordination mode of Eu^{3+} and asymmetry unit. (b) Second building units. (c) "Eu–O–C" chains along the *a* axis. (d) The layered structure of the Eu-MOF.

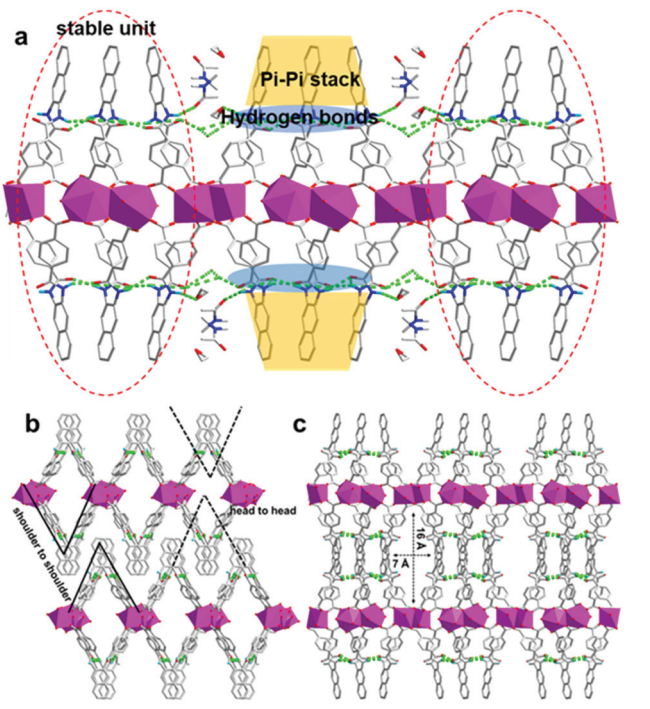

Fig. 2 (a) Hydrogen bonding interactions and π–π stacking interactions every layer. (b) The stack way of layers. (c) 3D structure viewing along *c* axis.

"O═C–NH" groups between adjacent stable units are linked with H_2O molecules and DMAC molecules by hydrogen bonding interactions (Fig. 2a). And the hydrogen bonding interactions are: O–H···O d = 2.78 Å, θ = 170°; N–H···O d = 2.74–2.81 Å, and θ = 147–156°. The hydrogen bonding interactions between stable units and solvent molecules can collaborate with stable units. On the one hand, the stable units relying on supramolecular interactions strengthen the stability of every layer. On the other hand, the stable units promoted that the "V" shaped ligands in the adjacent layers are stacked by shoulder to shoulder rather than head to head (Fig. 2b). If the "V" shaped ligands in the adjacent layers stacked by head to head, the pore channels in the layers would be occupied by the heads of the ligands(naphthalene groups). At last, adjacent layers stack by hydrogen bonding and van der Waals force between solvents and ligands while new diamond pore channels (7 Å × 16 Å) appear after stacking (Fig. 2c).

It is worth emphasizing that the crystallization process of the Eu-MOF not only relies on coordination bonding interactions but is also influenced by hydrogen bonding interactions and π–π stacking interactions. In particular, stable units appear in an assembled process as a special type of building unit, larger than the second building units, resulting from the promotion of supramolecular interactions. Interestingly, functional groups of ligands play multiple roles in the assembled progress of the Eu-MOF. The "O═C–NH" groups not only provide hydrogen bonding interactions for the stable units but can also be used as hydrogen bonding sites combined with solvent molecules. After careful analysis, two thirds of them provide structural support for the stable units and the rest of them can interact with solvent molecules to promote the stack of 2D layers. Similarly, the naphthalene groups not only can stabilize the small units by π–π stacking interactions but can also control the layers how to stack by the steric hindrance effect. The above analysis proved that the crystal structure we expected were obtained by designing functional ligands and the design strategy is effective. Thus, the ingenious structure encouraged us to carry out the subsequent study about properties of the Eu-MOF.

PXRD and thermal stability

As displayed in Fig. S4,† the experimental PXRD patterns of the Eu-MOF are in accordance with the simulated ones, indicating that the Eu-MOF was synthesized in a highly pure phase. At the same time, the Tb-MOF and Gd-MOF are isostructural with the Eu-MOF. Through the thermal stability under N_2 atmosphere from 30 to 800 °C, the Ln-MOFs lost free DMAC molecules and H_2O molecules in the pore channels firstly, causing a weight loss of around 14% before 340 °C. Then the weight of the Ln-MOF decreased around 6% at 390 °C, resulting from the removal of coordinated H_2O and DMAC. Finally, structural collapse occurred gradually while temperature increased above 400 °C (Fig. S5†). In conclusion, the synthesized Ln-MOFs are thermally stable enough to be investigated in a common environment.

Photoluminescence properties

First, the excited states of the free ligand were calculated and listed in Table S3† and the optimized geometry of the free ligand was displayed in Fig. S7† according to time-dependent density functional theory (DFT). The single excited state was calculated as 18 689 cm^{-1} and the first triple excited state was calculated as 11 913 cm^{-1}. The calculated results suggested the ligand might have too excited state levels for sensitizing Eu^{3+} effectively, encouraging us to synthesize the ligand and the Eu-MOF. Then the photoluminescence properties of the ligand and the Eu-MOF were studied by a steady-state fluorescence spectrometer. As we observed in Fig. S6,† the ligand excited by UV light can emit a strong turquoise fluorescence at 472 nm, originating from the intramolecular and intermolecular π*–π transitions. In the presence of naphthalene groups, the delocalized electrons increased while the excited energy levels of the ligand might be not high. Interestingly, the solid luminescence spectrum of the Eu-MOF showed f–f transitions ($^5D_0$–$^7F_0$, $^5D_0$–$^7F_1$, $^5D_0$–$^7F_2$, $^5D_0$–$^7F_3$, and $^5D_0$–$^7F_4$) and π*–π transitions at the same time (Fig. S8 and S9†), suggesting the incomplete "antenna effect". Unfortunately, the luminescence spectrum of Tb-MOF only shows π–π* transitions of the ligand at 468 nm and no f–f transitions of Tb^{3+} (Fig. S10†), caused by low excited energy levels of the ligand. Similarly, the Gd-MOF excited by UV light also emits cyan luminescence, resulting from π–π* transitions of the ligand (Fig. S10†). In order to illuminate the luminescence difference of the Ln-MOF, the S_1 (26 667 cm^{-1}, 375 nm) and T_1 (20 618 cm^{-1}, 485 nm) of the ligand were measured by the UV-Vis absorption spectrum of the ligand and phosphorescence spectrum of the Gd-MOF at 77 K (Fig. S8†). According to Reinhold's empirical rule,[50–52] intersystem crossing would occur effectively if the energy gap (ΔE_1) between S_1 and T_1 of a ligand is larger than 5000 cm^{-1}. The ΔE_1 of our ligand is 6049 cm^{-1} a little more than 5000 cm^{-1}. As reported,[53,54] the energy transfer effectively from a ligand to Eu^{3+} when the energy gap (ΔE_2) between T_1 of a ligand and $^5D_0$ of Eu^{3+} is not lower than 3000 cm^{-1}. But the ΔE_2 between the ligand and Eu^{3+} is 3118 cm^{-1} close to 3000 cm^{-1}. As displayed in Fig. 3, the path I and II occurred inefficiently in the luminescence process of the Eu-MOF. Thus, the Eu-MOF shows two emissions, including fluorescence at 471 nm of the

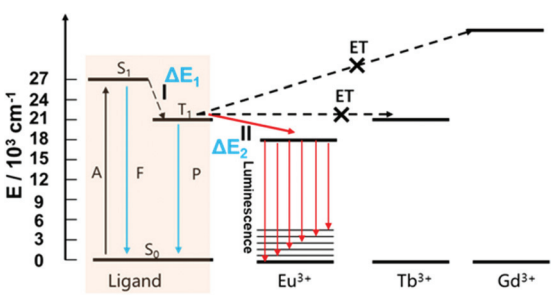

Fig. 3 The luminescence mechanism of the Eu-MOF (A: absorption; F: fluorescence; P: phosphorescence; I: intersystem crossing; II: energy transfer between T_1 of ligand and $^5D_0$ of Eu^{3+}).

ligand and luminescence at 614 nm of Eu^{3+}. And the luminescence quantum yield (Φ) is 1.02%. In a summary, the Eu-MOF possessing two luminescent centers is still worth exploring in luminescent sensors although the ligand cannot sensitize Eu^{3+} absolutely. In summary, the Eu-MOF possessing two luminescent centers is still worth exploring in luminescent sensors although the ligand cannot sensitize Eu^{3+} absolutely.

Temperature sensing property of the Eu-MOF

Based on the fact that the Eu-MOF can emit two luminescence signals from Eu^{3+} and the ligand, the temperature sensing capacity of the Eu-MOF was studied and the testing results suggested that the Eu-MOF can be developed as ratiometric luminescence thermometers at low and high temperatures. The Eu-MOF was excited by a 365 nm UV light and the luminescence spectra were recorded as shown in Fig. 4a while the environmental temperature ranged from 120 K to 400 K. It is worth noticing that Eu^{3+} emitted an obviously weaker luminescence at 616 nm with the increasing temperature while the fluorescence intensity of the ligands at 471 nm declined slightly. The comparison of the descent speed of the luminescence emission intensity are shown in Fig. 4b where the luminescence intensities of Eu^{3+} at 616 nm and the ligand at 471 nm show the respective decrease rates of 0.35% per K and 0.27% per K from 120 K to 400 K. The different decrease rates were caused by the difference of the energy loss pathway that the decreased luminescence intensity of Eu^{3+} resulted from the stronger energy-back transfer from Eu^{3+} to the organic ligand while the declined luminescence intensity of the organic ligands was mainly caused by the pathway of thermal enhanced resonance. Inspired by the fact that the luminescence intensity of Eu^{3+} decreased faster, we thought the luminescence intensity of the organic ligands (I_L, 471 nm) and the Eu^{3+} luminescence intensity (I_{Eu}, 616 nm) might be calculated as a ratiometric parameter ($\Delta = I_L/I_{Eu}$) monitoring temperature. Besides, in the single-lanthanide MOF Eu-MOF, two luminescent centers have a high correlation and the changing trend of the temperature parameter ($\Delta = I_L/I_{Eu}$) can be explained by the following equation (Boltzmann law).

$$\Delta = A\exp\left(\frac{-\Delta E}{K_B T}\right) + B \quad (1)$$

where ΔE represents the threshold value when the energy transfer occurs effectively between organic ligands and Eu^{3+}; K_B represents the Boltzmann constant (1.380649×10 J K^{-1}); T represents the Kelvin temperature; A and B represent the constant. The experimental results are given in Fig. 4c where the practical Δ for the Eu-MOF can be well explained by eqn (2).

$$\Delta = 654.76\exp\left(\frac{-3131.77}{T}\right) + 0.03 \quad (2)$$

With the correlation coefficient $R^2 = 0.996$. The fitted result means the validity of the eqn (1) and suggests the existence of two energy loss pathways in the Eu-MOF. The threshold value ΔE of the Eu-MOF was 2174.18 cm^{-1} according to the fitted results, which is in accordance with the ΔE_2.

Relative sensitivity (S_r) is an important parameter for evaluating the capacity of the sensing temperature and can eliminate the influence of different temperature parameters. The relative sensitivity be calculated using the following defined eqn (3).

$$S_r = \frac{\left(\left|\frac{\partial \Delta}{\partial T}\right|\right)}{\Delta} \quad (3)$$

where Δ represents the experimental temperature parameter (I_L/I_{Eu}) and T is the absolute temperature. On the basis of the defined eqn (3), the max S_r of the Eu-MOF is 2.73% K^{-1} at 400 K (Fig. 5a). Although many lanthanide MOF luminescence thermometers have been reported so far, single-lanthanide MOFs with higher relative sensitivity in the range of 120 K to 400 K are rarely reported (Table S4†). As listed in the Table S4,† our Eu-MOF's relative sensitivity is above-average.

Temperature uncertainty (δT) is also one of important factors for assessing the quality of luminescence thermometers. It represents the smallest value of the change of temperature parameters (Δ) when the intrinsic errors of the instruments occur. It can be calculated using the following eqn (4):

$$\delta T = \frac{1}{S_r}\frac{\delta \Delta}{\Delta} \quad (4)$$

where $\delta\Delta/\Delta$ is the intrinsic relative uncertainty caused by the instruments (mainly including: CCD and PMT fluorescence detectors), the value of $\delta\Delta/\Delta$ can reach around 0.03%. S_r is the

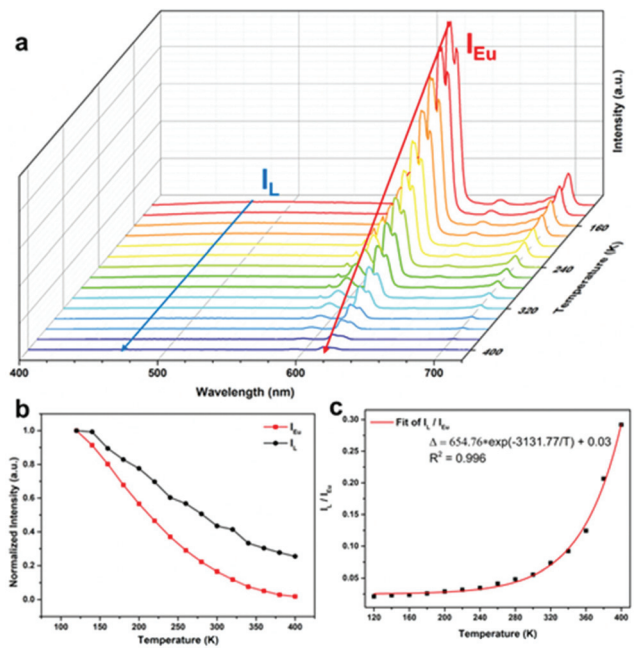

Fig. 4 (a) Emission spectra (λ_{ex} = 365 nm) of the Eu-MOF in the temperature range of 120–400 K (b) The changing trend of the luminescence intensity (I_{ligand} and I_{Eu}). (c) The measured temperature parameters ($\Delta = I_L/I_{Eu}$) and the fitted line by Boltzmann law.

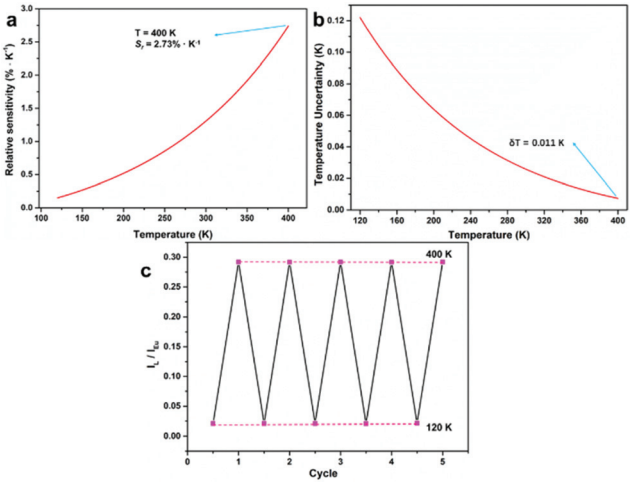

Fig. 5 (a) The relative sensitivity (S_r) of the Eu-MOF. (b) The temperature uncertainty (δT) of the Eu-MOF. (c) The reversible emission intensity ratio (I_L/I_{Ln}) of the Eu-MOF between 120 K and 400 K.

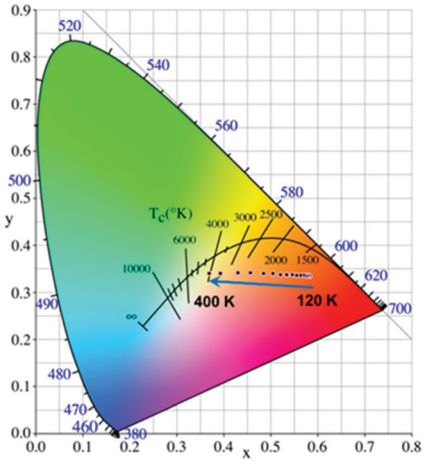

Fig. 6 The CIE chromaticity coordinates of the Eu-MOF in the increasing temperature process.

relative sensitivity of our Eu-MOF. And the least value of ΔT for the Eu-MOF is calculated to be 0.011 K (Fig. 5b).

The repeatability (R) is another important indicator for evaluating the performance of luminescence thermometers and was calculated using the following equation:

$$R = 1 - \frac{\max|\Delta_a - \Delta_i|}{\Delta} \quad (5)$$

where Δ_a represents the average value of the temperature parameters (I_L/I_{Eu}) extracted from the calibration curve, and Δ_i represents each measurement value of the temperature measurement parameter. It is observed that no obvious hysteresis occurr when the temperature increases and decreases repeatedly. According to eqn (5), the R value of the temperature parameter can reach more than 95% when the temperature increaes and decreases for five times between 120 K and 400 K (Fig. 5c). Moreover, the Eu-MOF retained the structural integrity after the temperature cycled test, which was proved by the PXRD of the sample before and after heating (Fig. S4†).

As a single-lanthanide MOF luminescence ratio-thermometer, the Eu-MOF can achieve the change of the luminescence color ranging from red (120 K) to white (400 K) with increasing temperature (Fig. 6), which is caused by the fact that the luminescence intensity of Eu^{3+} decrease faster than the ligand. So our Eu-MOF has the potential of monitoring the temperature (120–400 K) by the CIE coordinates.

Detection of picric acid

Firstly, the luminescence behavior of the Eu-MOF dispersed in an common organic solvent (DMAC, DMF, methanol, ethanol, THF, dichloromethane, 1,4-dioxane, acetonitrile, acetone, and isopropanol) was investigated (Fig. S11†). The Eu-MOF (2 mg) after grinding was added in the organic solution (2 mL) and was treated under ultrasonication. The uniformly dispersed turbid liquids were excited by UV light and the luminescence spectra were recorded respectively. As displayed in Fig. S11,† the luminescence intensity of the Eu-MOF in DMAC is higher than others while the Eu-MOF in acetone shows a weaker emission than others. Besides, most of the nitro explosives can be dissolved in DMAC and so DMAC was used as a detection environment. Then, the performance of the Eu-MOF detecting picric acid was studied step by step. First of all, the Eu-MOF was dispersed finely in DMAC by repeating the previous operation and the uniform suspension was obtained as the detection reagent. Then six kinds nitro organic compounds (PA, *p*-nitrophenol, 3-nitroaniline, *m*-dinitrobenzene, nitrobenzene, and *p*-nitrotoluene) were added into the detection reagents respectively till the concentration of 0.1 mM was reached and the luminescence intensity of Eu^{3+} at 616 nm was recorded (λ_{ex} = 365 nm). Comparing the luminescence intensity of the mixture at 616 nm in Fig. 7, we observed that our detection reagent showed the weakest emission after being mixed with

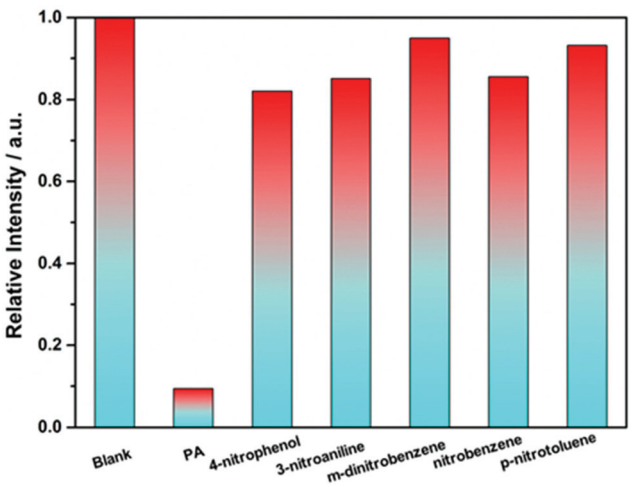

Fig. 7 Luminescence responses of the Eu-MOF in various nitro explosives (0.1 mM) in DMAC.

PA. On the basis of the change of the luminescence intensity in Fig. 7, it can be concluded that the Eu-MOF has the capability of detecting nitro explosives especially PA. Thus, the titration experiments of these nitro explosives were carried out to precisely evaluate the sensitivity of the detection reagent. The experimental results for PA were displayed in Fig. 8a, it is obvious that the luminescence intensity at 616 nm showed a gradient descent with the increased concentration of PA from 0 to 0.1 mM. As shown in Fig. 8b, the luminescence intensity at 616 nm was recorded respectively for every concentration of PA and the experimental points were fitted with a linear model. The fitted result are in accordance with the following Stern–Volmer (SV) equation.

$$I_0/I = 1 + K_{SV}[M] \quad (6)$$

where I_0 is the initial luminescence intensity at 616 nm, I is the luminescence intensity after being mixed with nitro explosives, [M] represents the concentration of the quencher, K_{SV} can be used for assessing the sensitivity of the detection reagent. As displayed in Fig. 8b, the fitted line shows a satisfactory correlation (R^2 = 0.9916) at a low concentration range (0–0.04 mM). Surprisingly, the K_{SV} reached 53 339 M^{-1}, which means that our Eu-MOF might take the leading position among the luminescent MOFs detecting picric acid (Table S5†). Besides, the detection limit was lower than 0.005 mM according to distinguishing emission spectra shown in Fig. 8a. The experimental results of other nitro explosives were listed in the following Table S6 and Fig. S12–S16.†

The detection sensitivity order was as follows: picric acid > *p*-nitrophenol > 3-nitroaniline > *m*-dinitrobenzene > *p*-nitrotoluene > nitrobenzene, which proved that the Eu-MOF can be used for detecting PA. And it is also important for the detection reagent to be used and cycled repeatedly. Thus, the Eu-MOF after being mixed with 0.1 mM PA was washed by DMAC and used for detecting PA after centrifugation. As showed in Fig. S17,† the cycling number of the Eu-MOF reached at least five. At the same time, the reclaimed Eu-MOF retained the structural integrity, which was proved by the PXRD and SEM image of Eu-MOF after detecting PA (Fig. S4 and S20†).

Although the above content has showed that our Eu-MOF is an excellent sensor for detecting PA, it is necessary to investigate the detection mechanism. The kinds of reasons causing the lower luminescence intensity of the Eu-MOF, including: structural collapse, competitive absorption, photoinduced electron transfer (PET), and fluorescence resonance energy transfer (FRET). The structural collapse was excluded firstly according to above cycling experiment. Secondly, it is observed obviously that the PA showed a high absorbance intensity at 365 nm (Fig. S18†) and it can be concluded that competitive absorption occurred between the Eu-MOF and PA. Then it can be confirmed that PET is also one of reasons causing luminescence quenching, because the fluorescence lifetime at 616 nm of the Eu-MOF became shorter after being mixed with PA (Fig. S19†). Finally, the emission of the Eu-MOF at 617 nm did not overlap with the absorption spectrum of PA (Fig. 8 and Fig. S18†), so it can be inferred that FRET did not play a role in the quenching process. In conclusion, competitive absorption and PET played an important role in quenching the luminescence of Eu-MOF when PA molecules were gathered by hydrogen bond sites of the Eu-MOF.

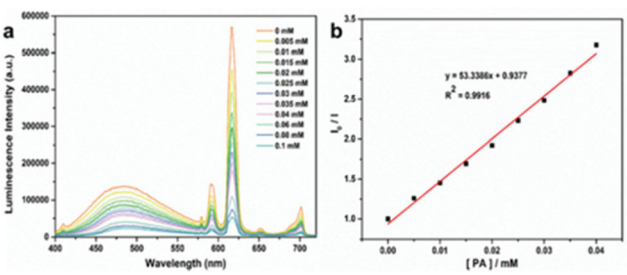

Fig. 8 (a) The luminescence spectra of the Eu-MOF recorded with different concentrations of PA (0–0.1 mM) in DMAC. (b) SV plot of I_0/I *vs.* increasing concentrations of PA.

Conclusions

In conclusion, we designed and synthesized a dual-emitting and multi-functional Eu-MOF by structural design and energy level regulation of the ligand. Structure analysis revealed that the Eu-MOF has two types of diamond pore channels caused by the stack of the layers and surrounded by the "V" shaped ligands in the layers respectively. And the "O═C–NH" groups as hydrogen bonding sites not only can build hydrogen bonds in the layers but can also interact with the substrate as recognition sites. Photoluminescence properties of the Ln-MOF (Ln = Eu, Tb, Gd) and luminescence mechanism of the dual-emitting Eu-MOF were studied. The temperature-dependent photoluminescence properties of the Eu-MOF were studied and the results suggested that the Eu-MOF excited at 365 nm can achieve the luminescence color change from red to white in the temperature range from 120 K to 400 K. Besides, the Eu-MOF could detect PA selectively and effectively and the Ksv reached 53 339 M^{-1}. Our work proved that the designed strategy can construct multi-functional and dual-emitting single-lanthanide MOFs, providing more choices for the design and application of single-lanthanide MOFs.

Author contributions

W. L. gave ideas, Xg. L. prepared the ligand and single crystal of the Eu-MOF, Y. K. carried out the temperature sensing experiments, Xs. Y. and Zh. J. carried out other experiments. Also Xg. L. organized the above experiments and wrote the manuscript and supplemented it with the guidance of W. L. and Ws. L.

Conflicts of interest

All authors declare no competing financial interest.

Acknowledgements

This work was supported by the National Natural Science Foundation of China (Grant No. 21871122 and 21901095), the Gansu Planning Projects on Science and Technology (21JR7RA512) and the Fundamental Research Funds for the Central Universities (Grant No. lzujbky-2021-8, lzujbky-2021-kb06, and lzujbky-2021-kb17).

References

1 E. Chapman, S. Ullah, H. Wang, L. Feng, K. Wang, H.-C. Zhou, J. Li, T. Thonhauser and K. Tan, Tuning the Adsorption Properties of Metal-Organic Frameworks through Coadsorbed Ammonia, *ACS Appl. Mater. Interfaces*, 2021, **13**, 43661–43667.

2 P.-Q. Liao, N.-Y. Huang, W.-X. Zhang, J.-P. Zhang and X.-M. Chen, Controlling guest conformation for efficient purification of butadiene, *Science*, 2017, **356**, 1193–1196.

3 J. Pei, K. Shao, J.-X. Wang, H.-M. Wen, Y. Yang, Y. Cui, R. Krishna, B. Li and G. Qian, A Chemically Stable Hofmann-Type Metal-Organic Framework with Sandwich-Like Binding Sites for Benchmark Acetylene Capture, *Adv. Mater.*, 2020, **32**, e1908275.

4 Y. Qiao, X. Chang, J. Zheng, M. Yi, Z. Chang, M.-H. Yu and X.-H. Bu, Self-Interpenetrated Water-Stable Microporous Metal–Organic Framework toward Storage and Purification of Light Hydrocarbons, *Inorg. Chem.*, 2021, **60**, 2749–2755.

5 Z. Xu, X. Xiong, J. Xiong, R. Krishna, L. Li, Y. Fan, F. Luo and B. Chen, A robust Th-azole framework for highly efficient purification of C_2H_4 from a $C_2H_4/C_2H_2/C_2H_6$ mixture, *Nat. Commun.*, 2020, **11**, 3163.

6 L. Jiao, R. Zhang, G. Wan, W. Yang, X. Wan, H. Zhou, J. Shui, S.-H. Yu and H.-L. Jiang, Nanocasting SiO_2 into metal-organic frameworks imparts dual protection to high-loading Fe single-atom electrocatalysts, *Nat. Commun.*, 2020, **11**, 2831.

7 Y. Sun, Z. Xue, Q. Liu, Y. Jia, Y. Li, K. Liu, Y. Lin, M. Liu, G. Li and C.-Y. Su, Modulating electronic structure of metal-organic frameworks by introducing atomically dispersed Ru for efficient hydrogen evolution, *Nat. Commun.*, 2021, **12**, 1369–1376.

8 C.-P. Wang, Y. Feng, H. Sun, Y. Wang, J. Yin, Z. Yao, X.-H. Bu and J. Zhu, Self-Optimized Metal–Organic Framework Electrocatalysts with Structural Stability and High Current Tolerance for Water Oxidation, *ACS Catal.*, 2021, **11**, 7132–7143.

9 T. Yan, J.-H. Guo, Z.-Q. Liu and W.-Y. Sun, Metalloporphyrin Encapsulation for Enhanced Conversion of CO_2 to C_2H_4, *ACS Appl. Mater. Interfaces*, 2021, **13**, 25937–25945.

10 J.-H. Zhang, W. Yang, M. Zhang, H.-J. Wang, R. Si, D.-C. Zhong and T.-B. Lu, Metal-organic layers as a platform for developing single-atom catalysts for photochemical CO_2 reduction, *Nano Energy*, 2021, **80**, 105542.

11 T. Grancha, J. Ferrando-Soria, J. Cano, P. Amorós, B. Seoane, J. Gascon, M. Bazaga-García, E. R. Losilla, A. Cabeza, D. Armentano and E. Pardo, Insights into the Dynamics of Grotthuss Mechanism in a Proton-Conducting Chiral bio MOF, *Chem. Mater.*, 2016, **28**, 4608–4615.

12 A. B. Kanj, A. Chandresh, A. Gerwien, S. Grosjean, S. Bräse, Y. Wang, H. Dube and L. Heinke, Proton-conduction photomodulation in spiropyran-functionalized MOFs with large on–off ratio, *Chem. Sci.*, 2020, **11**, 1404–1410.

13 X. Li, H. Zhang, H. Yu, J. Xia, Y.-B. Zhu, H.-A. Wu, J. Hou, J. Lu, R. Ou, C. D. Easton, C. Selomulya, M. R. Hill, L. Jiang and H. Wang, Unidirectional and Selective Proton Transport in Artificial Heterostructured Nanochannels with Nano-to-Subnano Confined Water Clusters, *Adv. Mater.*, 2020, **32**, e2001777.

14 I. Stassen, N. Burtch, A. Talin, P. Falcaro, M. Allendorf and R. Ameloot, An updated roadmap for the integration of metal-organic frameworks with electronic devices and chemical sensors, *Chem. Soc. Rev.*, 2017, **46**, 3185–3241.

15 S.-N. Zhao, Y. Zhang, S.-Y. Song and H.-J. Zhang, Design strategies and applications of charged metal organic frameworks, *Coord. Chem. Rev.*, 2019, **398**, 113007.

16 L. Chen, H.-F. Wang, C. Li and Q. Xu, Bimetallic metal-organic frameworks and their derivatives, *Chem. Sci.*, 2020, **11**, 5369–5403.

17 G. E. Gomez, R. Marin, A. N. Carneiro Neto, A. M. P. Botas, J. Ovens, A. A. Kitos, M. C. Bernini, L. D. Carlos, G. J. A. A. Soler-Illia and M. Murugesu, Tunable Energy-Transfer Process in Heterometallic MOF Materials Based on 2,6-Naphthalenedicarboxylate: Solid-State Lighting and Near-Infrared Luminescence Thermometry, *Chem. Mater.*, 2020, **32**, 7458–7468.

18 J. González, P. Sevilla, G. Gabarró-Riera, J. Jover, J. Echeverría, S. Fuertes, A. Arauzo, E. Bartolomé and E. C. Sañudo, A Multifunctional Dysprosium-Carboxylato 2D Metall-Organic Framework, *Angew. Chem., Int. Ed.*, 2021, **60**, 12001–12006.

19 H. Liu, Y. Liu, Y. Meng, X. Shi, J. Sun, L. Zhao, D. Chen, H. Hao, D. Li, J. Dou and J. Han, Di-functional luminescent sensors based on Y^{3+} doped Eu^{3+} and Tb^{3+} coordination polymers: fast response and visible detection of Cr^{3+} Fe^{3+} ions in aqueous solutions and acetone, *RSC Adv.*, 2020, **10**, 32232–32240.

20 P. F. Muldoon, G. Collet, S. V. Eliseeva, T.-Y. Luo, S. Petoud and N. L. Rosi, Ship-in-a-Bottle Preparation of Long Wavelength Molecular Antennae in Lanthanide Metal-Organic Frameworks for Biological Imaging, *J. Am. Chem. Soc.*, 2020, **142**, 8776–8781.

21 S. Sun, C. Wei, Y. Xiao, G. Li and J. Zhang, Zirconium-based metal–organic framework gels for selective luminescence sensing, *RSC Adv.*, 2020, **10**, 44912–44919.

22 S. Xing and C. Janiak, Design and properties of multiple-emitter luminescent metal-organic frameworks, *Chem. Commun.*, 2020, **56**, 12290–12306.

23 S. N. Zhao, L. J. Li, X. Z. Song, M. Zhu, Z. M. Hao, X. Meng, L. L. Wu, J. Feng, S. Y. Song, C. Wang and H. J. Zhang,

Lanthanide Ion Codoped Emitters for Tailoring Emission Trajectory and Temperature Sensing, *Adv. Funct. Mater.*, 2015, **25**, 1463–1469.

24 Z. Cui, X. Zhang, S. Liu, L. Zhou, W. Li and J. Zhang, Anionic Lanthanide Metal-Organic Frameworks: Selective Separation of Cationic Dyes, Solvatochromic Behavior, and Luminescent Sensing of Co(II) Ion, *Inorg. Chem.*, 2018, **57**, 11463–11473.

25 Y. Kitagawa, M. Tsurui and Y. Hasegawa, Bright red emission with high color purity from Eu(iii) complexes with π-conjugated polycyclic aromatic ligands and their sensing applications, *RSC Adv.*, 2021, **12**, 810–821.

26 H.-Y. Li, S.-N. Zhao, S.-Q. Zang and J. Li, Functional metal-organic frameworks as effective sensors of gases and volatile compounds, *Chem. Soc. Rev.*, 2020, **49**, 6364–6401.

27 T. Liang, Z. Guo, Y. He, Y. Wang, C. Li, Z. Li and Z. Liu, Cyanine-Doped Lanthanide Metal-Organic Frameworks for Near-Infrared II Bioimaging, *Adv. Sci.*, 2022, **9**, e2104561.

28 S. Ma, D. Yuan, X.-S. Wang and H.-C. Zhou, Microporous lanthanide metal-organic frameworks containing coordinatively linked interpenetration: syntheses, gas adsorption studies, thermal stability analysis, and photoluminescence investigation, *Inorg. Chem.*, 2009, **48**, 2072–2077.

29 Q. Tang, S. Liu, Y. Liu, D. He, J. Miao, X. Wang, Y. Ji and Z. Zheng, Color tuning and white light emission via in situ doping of luminescent lanthanide metal-organic frameworks, *Inorg. Chem.*, 2014, **53**, 289–293.

30 Z. Wang, C.-Y. Zhu, Z.-W. Wei, Y.-N. Fan and M. Pan, Breathing-Ignited Long Persistent Luminescence in a Resilient Metal-Organic Framework, *Chem. Mater.*, 2020, **32**, 841–848.

31 Z. Xiaoxiong, Z. Wenjun, L. Cuiliu, Q. Xiaohong and Z. Chengyu, Eu^{3+}-Postdoped UIO-66-Type Metal-Organic Framework as a Luminescent Sensor for Hg^{2+} Detection in Aqueous Media, *Inorg. Chem.*, 2019, **58**, 3910–3915.

32 W. Xie, J.-S. Qin, W.-W. He, K.-Z. Shao, Z.-M. Su, D.-Y. Du, S.-L. Li and Y.-Q. Lan, Encapsulation of an iridium complex in a metal-organic framework to give a composite with efficient white light emission, *Inorg. Chem. Front.*, 2017, **4**, 547–552.

33 B. Yan, Luminescence response mode and chemical sensing mechanism for lanthanide-functionalized metal-organic framework hybrids, *Inorg. Chem. Front.*, 2021, **8**, 201–233.

34 X. Z. Song, S. Y. Song, S. N. Zhao, Z. M. Hao, M. Zhu, X. Meng, L. L. Wu and H. J. Zhang, Single-Crystal-to-Single-Crystal Transformation of a Europium(III) Metal-Organic Framework Producing a Multi-responsive Luminescent Sensor, *Adv. Funct. Mater.*, 2014, **24**, 4034–4041.

35 T. Wu, Z. Y. Jiang, X. B. Xue, S. C. Wang, M. Z. Chen, J. Wang, H. S. Liu, J. Yan, Y. S. Chan and P. S. Wang, Molecular hexagram and octagram: Position determined 3D metallo-supermolecules and concentration-induced transformation, *Chin. Chem. Lett.*, 2021, **32**, 1911–1914.

36 J. H. Fu, S. Y. Wang, Y. S. Chen, S. Prusty and Y. T. Chan, One-Pot Self-Assembly of Stellated Metallosupramolecules from Multivalent and Complementary Terpyridine-Based Ligands, *J. Am. Chem. Soc.*, 2019, **141**, 16217–16221.

37 L. J. Han, W. Yan, S. G. Chen, Z. Z. Shi and H. G. Zheng, Exploring the Detection of Metal Ions by Tailoring the Coordination Mode of V-Shaped Thienylpyridyl Ligand in Three MOFs, *Inorg. Chem.*, 2017, **56**, 2936–2940.

38 H. Q. Jin, J. N. Xu, L. Y. Zhang, B. Ma, X. X. Shi, Y. Fan and L. Wang, Multi-responsive luminescent sensor based on Zn(II) metal-organic framework for selective sensing of Cr(III), Cr(VI) ions and p-nitrotolune, *J. Solid State Chem.*, 2018, **268**, 168–174.

39 Y. Liu, L. Liu, X. Chen, Y. Liu, Y. Han and Y. Cui, Single-Crystalline Ultrathin 2D Porous Nanosheets of Chiral Metal-Organic Frameworks, *J. Am. Chem. Soc.*, 2021, **143**, 3509–3518.

40 Y. Cui, B. Chen and G. Qian, Lanthanide metal-organic frameworks for luminescent sensing and light-emitting applications, *Coord. Chem. Rev.*, 2014, **273**, 76–86.

41 Y. Cui, B. Li, H. He, W. Zhou, B. Chen and G. Qian, Metal–Organic Frameworks as Platforms for Functional Materials, *Acc. Chem. Res.*, 2016, **49**, 483–493.

42 Y. Cui, H. Xu, Y. Yue, Z. Guo, J. Yu, Z. Chen, J. Gao, Y. Yang, G. Qian and B. Chen, A Luminescent Mixed-Lanthanide Metal–Organic Framework Thermometer, *J. Am. Chem. Soc.*, 2012, **134**, 3979–3982.

43 Y. Cui, Y. Yue, G. Qian and B. Chen, Luminescent Functional Metal–Organic Frameworks, *Chem. Rev.*, 2012, **112**, 1126–1162.

44 X. Rao, T. Song, J. Gao, Y. Cui, Y. Yang, C. Wu, B. Chen and G. Qian, A Highly Sensitive Mixed Lanthanide Metal–Organic Framework Self-Calibrated Luminescent Thermometer, *J. Am. Chem. Soc.*, 2013, **135**, 15559–15564.

45 T. S. Wang, N. Zhang, R. K. Bai and Y. Y. Bao, Aggregation-enhanced FRET-active conjugated polymer nanoparticles for picric acid sensing in aqueous solution, *J. Mater. Chem. C*, 2018, **6**, 266–270.

46 B. Jiang, W. Liu, S. Liu and W. Liu, Coumarin-encapsulated MOF luminescence sensor for detection of picric acid in water environment, *Dyes Pigm.*, 2021, **184**, 108794.

47 W. Liu, C. Chen, Z. Wu, Y. Pan, C. Ye, Z. Mu, X. Luo, W. Chen and W. Liu, Construction of Multifunctional Luminescent Lanthanide MOFs by Hydrogen Bond Functionalization for Picric Acid Detection and Fluorescent Dyes Encapsulation, *ACS Sustainable Chem. Eng.*, 2020, **8**, 13497–13506.

48 S. K. Sachan and G. Anantharaman, Cuboctahedral [In-36(mu-OH)(24)(NO_3)(8)(Imtb)(24)]MOF with Atypical Pyramidal Nitrate Ion in SBU: Lewis Acid-Base Assisted Catalysis and Nanomolar Sensing of Picric Acid, *Inorg. Chem.*, 2021, **60**, 9238–9242.

49 Y. Zou, K. Huang, X. Zhang, D. Qin and B. Zhao, Tetraphenylpyrazine-Based Manganese Metal Organic Framework as a Multifunctional Sensor for Cu^{2+}, Cr^{3+}, MnO^{4-}, and 2,4,6-Trinitrophenol and the Construction of a

Molecular Logical Gate, *Inorg. Chem.*, 2021, **60**, 11222–11230.

50 F. J. Steemers, W. Verboom, D. N. Reinhoudt, E. B. van der Tol and J. W. Verhoeven, New Sensitizer-Modified Calix[4]arenes Enabling Near-UV Excitation of Complexed Luminescent Lanthanide Ions, *J. Am. Chem. Soc.*, 1995, **117**, 9408–9414.

51 S. Wu, Y. Lin, J. Liu, W. Shi, G. Yang and P. Cheng, Rapid Detection of the Biomarkers for Carcinoid Tumors by a Water Stable Luminescent Lanthanide Metal–Organic Framework Sensor, *Adv. Funct. Mater.*, 2018, **28**, 1707169.

52 H.-Q. Yin, X.-Y. Wang and X.-B. Yin, Rotation Restricted Emission and Antenna Effect in Single Metal–Organic Frameworks, *J. Am. Chem. Soc.*, 2019, **141**, 15166–15173.

53 X. G. Yang, X. Q. Lin, Y. B. Zhao, Y. S. Zhao and D. P. Yan, Lanthanide Metal-Organic Framework Microrods: Colored Optical Waveguides and Chiral Polarized Emission, *Angew. Chem., Int. Ed.*, 2017, **56**, 7853–7857.

54 Y. Liu, M. Pan, Q. Y. Yang, L. Fu, K. Li, S. C. Wei and C. Y. Su, Dual-Emission from a Single-Phase Eu-Ag Metal-Organic Framework: An Alternative Way to Get White-Light Phosphor, *Chem. Mater.*, 2012, **24**, 1954–1960.